

On the characterization of transiting exoplanets and magnetic spots with optical interferometry

R.Ligi¹, D. Mourard¹, A.-M. Lagrange², K. Perraut², A. Chiavassa¹

¹ Laboratoire Lagrange, UMR 7293 UNS-CNRS-OCA, Boulevard de l'Observatoire, CS 34229, 06304 NICE Cedex 4, France.
e-mail: roxanne.ligi@oca.eu

² UJF-Grenoble1/CNRS-INSU, Institut de Planétologie et d'Astrophysique de Grenoble, UMR 5274, Grenoble, F-38041, France

Received 16 April 2014; accepted 17 October 2014

ABSTRACT

Context. Stellar activity causes difficulties in the characterization of transiting exoplanets. In particular, magnetic spots are present on most exoplanet host stars, and they can lead to false detections with radial velocity, photometry or astrometry techniques. Studies have been performed to quantify their impact on infrared interferometry, but no such studies have been performed in the visible domain. This wavelength domain however allows reaching better angular resolution than the infrared one and is also the one mostly used for spectroscopic and photometric measurements.

Aims. We use a textbook case to make a complete analysis of the impact of an exoplanet and a spot on interferometric observables and relate it to current instruments capabilities, taking into account realistic achievable precisions.

Methods. We have built a numerical code called COMETS using analytical formulae to perform a simple comparison of exoplanets and spots' signals. We explore instrumental specificities needed to detect them, like the baseline length required, the accuracy and SNR. We also discuss the impact of exoplanets and spot's parameters on squared visibility and phase : exoplanet's diameter and size, exoplanet's position, spot's temperature, star's diameter.

Results. According to our study, the main improvement to bring is the sensitivity of instruments. The accuracy on squared visibilities has to be improved by a factor 10 to detect an exoplanet of 0.10 mas, leading to $< 0.5\%$ precision, along with phase measurements of $\sim 5^\circ$ accuracy beyond the first null of visibility. For a 0.05 mas exoplanet, accuracies of $\sim 0.1\%$ and $\sim 1^\circ$ from the first null are required on squared visibilities and phases, respectively. Magnetic spots can mimic these signals, leading to false exoplanet characterization. Phases measurements from the 3rd lobe is needed to disentangle between the spot and the exoplanet if they have the same radius.

Conclusions. By increasing interferometers sensitivity, more objects will become common between interferometric targets and photometric ones. Furthermore, new missions like PLATO, CHEOPS or TESS will provide bright exoplanets host stars. Measurements will thus overlap and provide a better characterization of stellar activity along with exoplanets's one.

Key words. stars: activity - techniques: interferometric - methods: numerical - stars: planetary systems

1. Introduction

The discovery of the first exoplanet around a solar type star by Mayor & Queloz (1995) has opened up a new field of research in both planetary and stellar sciences. The numerous exoplanets found up to now show a large variety of size, composition, distance from their host star, etc. that naturally raises the question of habitability along with the necessity of characterizing these new worlds. We have thus moved from the era of exoplanets discovery to the era of exoplanets characterization, which is closely related to the characterization of host stars.

When we observe an exoplanetary system, the measurements include both the exoplanetary signal and the stellar signal which depends on several parameters such as activity, rotation period, inclination, etc. We thus need to interpret these measurements and relate each signal to its physical origin to correctly detect or characterize the exoplanet signal.

Interferometry is actually of great interest in the direct characterization of exoplanets at many levels. It is a useful tool to exclude false-positive scenarii, which is a recurrent problem due to unresolved companions mimicking a planetary transit for *Kepler* candidates, as shown by Huber et al. (2012) for example. They performed interferometric observa-

tions with PAVO (Ireland et al. 2008) on CHARA to confirm the hypothesis of a planetary companion around Kepler-21. This exoplanet, discovered by Howell et al. (2012), is an Earth-like planet, and such exoplanets generally provoke smaller variations in RV measurements than stellar activity, which limits their detection. Beyond the validation of exoplanetary systems, interferometry has long been known as a possible way to detect light from exoplanets (Zhao et al. 2008; Monnier et al. 2004), but this remains still difficult at this time. In fact, some attempts to directly detect exoplanets with infrared interferometry have already been made. Matter et al. (2010) on AMBER/VLTI (Petrov & AMBER Consortium 2003) and MIDI/VLTI (Leinert et al. 2003), and Zhao et al. (2011) on MIRC/CHARA both tried to directly detect a planetary companion using respectively differential phase and closure phase measurements. Still, instrumental effects limit their detection (for both, a factor of 6 to 10 in the precision of the phase measurements has to be reached to detect the planetary signal) but improvements of their stability should provide better results in the future.

One of the difficulties encountered to achieve exoplanet characterization is to measure complex visibilities at advantageous spatial frequencies. This effect has been discussed by

Chelli et al. (2009) in a paper presenting the phase closure nulling method. They show that the effect of a faint companion is stronger around the visibility nulls of the primary. On phases, the companion's contribution remains constant as long as it is not resolved, including the frequencies of the primary nulls, and is even stronger than systematic errors. Duvert et al. (2010) applied this method to detect the 5-mag fainter companion of HD59717, and derived the mass and size of this binary system.

Finally, interferometry allows the measurement of many observables of a transiting planetary system through closure phases measurements. In particular, it allows to extract the inclination angle of the exoplanet (van Belle et al. 2008; Zhao et al. 2008) and other important parameters: impact parameter, transit velocity, stellar and planetary radius and transit ingress time (van Belle et al. 2008), making this technique a fundamental tool if no other data of the system is available.

In some cases, the presence of stellar spots can help determining exoplanets' properties, like their obliquity (Nutzman et al. 2011; Sanchis-Ojeda et al. 2011). In turn, exoplanet studies sometimes allow to detect and characterize a host star's spots and rotation (Silva-Valio & Lanza 2011). However, most of the time, stellar activity adds complexity to the analysis of the signals. Its characterization is thus necessary but not yet achievable, as show Baron et al. (2012) in the context of the Imaging Beauty Contest 2012.

The emergence of hypertelescopes constitutes an encouraging option to resolve this problem. It promises the direct imaging of transiting exoplanets and stellar surfaces (Labeyrie et al. 2012a,b) thanks to kilometric baselines and an important gain in the limiting magnitude of the instruments. Baines et al. (2007) demonstrated the interest of measuring the angular diameter of the star in transiting systems. We thus decided to focus our study on visible interferometric measurements of transiting systems, which has both scientific and technical great advantages. Since a star's photosphere is not perfectly symmetric and since we do not necessarily know the position of the transiting exoplanet at the time of the measurement, the information can only be extracted by crossing many data. This suggests the measurement of many visibilities and phases and the use of a (u, v) plane covering many directions. The advantage of the visible domain is first in the increased angular resolution for a given baseline, and second, the fact that it is the main domain used in photometry or in RV for indirect searches for planets. It is already used by several instruments that reach unprecedented angular resolution (up to 0.3 milliarcsecond): VEGA/CHARA (Mourard et al. 2009; Ligi et al. 2013), PAVO/CHARA (Ireland et al. 2008), VISION/NPOI (Armstrong et al. 1998). With the significant improvement in sensitivity and accuracy that visible interferometry has gained recently, it might be a good way to characterize spots and exoplanets signatures on interferometric observables and to disentangle the different signals.

In Section 2, we describe a new numerical code called COMETS allowing the modeling of interferometric observables of a star hosting a magnetic spot and/or a transiting exoplanet. We apply this code to analyze the impacts that exoplanets and spots' parameters produce on the minimum baselines length required to measure their signal in Section 3 and investigate their detectability in Section 3.4. We rise the question of the possibility to disentangle between spot and exoplanet in Section 4. We end by discussing the current interferometers' capabilities in detecting exoplanets in Section 5.

2. Models of the objects

COMETS (COde for Modeling ExoplaneT and Spots) is a numerical code using analytical formulae developed to model the interferometric observables (visibilities, closure phases or phases) provided by a star with a (dark) magnetic spot and/or a transiting exoplanet. The computation is made on a grid of a (u, v) plane with u and v ranging from $-1\text{ km}/\lambda$ to $1\text{ km}/\lambda$ with a step $du = dv$ smaller than $4m/\lambda$ (refined if necessary). We use a wavelength λ of 720 nm as used by VEGA instrument.

2.1. Representation of a transiting exoplanet

The star is represented by a linear limb-darkened (LD) disk of angular diameter θ_* obtained with the Claret coefficient b (Claret & Bloemen 2011) and maximum radius $\sigma_{\max} = \theta_*/2$. Its surface brightness distribution depends on its effective temperature $T_{\text{eff},*}$ and on the considered point at the stellar surface σ .

We consider the star centered at the origin of the coordinate system in the sky $\sigma_0 = (\alpha_0, \delta_0)$. The star's intensity I_* at any location point depends on an impact factor μ defined as $\mu = \sqrt{1 - \left(\frac{\sigma}{\sigma_{\max}}\right)^2}$. It represents the cosine of the angle formed by the line of sight and the normal to the surface at the considered point. Thus, the star's profile intensity can be written $I_*(\mu) = I_*(1) - b(1 - \mu)$ in a linear representation, where $I_*(1)$ is the star intensity at the centre of the star.

The contrast between a transiting exoplanet and its host star is very high in the optical domain (typically, the contrast is 10^{10} in the visible and $10^{6.5}$ in the infrared for Earth-like planets, see e.g. Traub & Jucks 2002). The transiting exoplanet located at any position $\sigma_p = (\alpha_p, \delta_p)$ on the stellar disk is thus assumed to be a dark disk of intensity $I_p = 0$ and angular diameter θ_p . Since the star is a LD disk, the star's intensity at the planet's location $I_*(\mu_p)$ precisely depends on the planet's location. Thus, the intensity profile of the system *star + planet* can be written:

$$I_*(\mu)\Pi_{(0,0,\theta)} - (I_*(\mu_p) - I_p)\Pi_{(\alpha_p,\delta_p,\theta_p)}, \quad (1)$$

where Π is the Gate function.

The complex visibility function represents the Fourier Transform of the surface brightness distribution of the source. Its calculations are detailed in Annex A.1. Since interferometers mainly measure the squared modulus of objects' visibilities, we have considered the squared modulus of the complex visibility in our study and its argument called the phase ϕ , described as $\phi = \tan^{-1}\left(\frac{\Im(V)}{\Re(V)}\right)$, where \Re and \Im respectively define the real and imaginary part of the complex number V . For a symmetric uniform disk representation, the amplitude of V follows Bessel function and decreases in the first lobe before reaching zero at $\theta B/\lambda = 1.22$ (called first null) where the phase jumps from 0 to $\pm\pi$. From the 2D complex visibility maps generated by COMETS, it is possible to estimate closure phases through the calculation of closure equation on any arbitrary triplet of (u, v) coordinates. This method has been recently used by Chiavassa et al. (2014). However, in the present study we decided to limit the analysis to the phase plane without calculating closure phase. This simplifies the calculation and is a good compromise with respect to the expected effects on the phase.

2.2. Representation of a spot

The spot is usually decomposed into two distinct parts, the umbra and the penumbra, of intensities I_{um} and I_{pen} respectively.

A spot located at the position $\sigma_s = (\alpha_s, \delta_s)$ on the stellar disk is represented by two superimposed disks both centered in σ_s with $\theta_{\text{pen}} > \theta_{\text{um}}$, θ_{um} and θ_{pen} being the angular diameters of the umbra and the penumbra respectively.

Thus, the intensity profile of the umbra is written $(I_\star(\mu_s) - I_{\text{um}}) \Pi_{(\alpha_s, \delta_s, \theta_{\text{um}}), \mu_s}$ representing the impact parameter at the spot's location. The intensity profile of the penumbra is written as the subtraction of two disks of intensity I_{pen} and angular diameters θ_{pen} and θ_{um} : $(I_\star(\mu_s) - I_{\text{pen}}) (\Pi_{(\alpha_s, \delta_s, \theta_{\text{pen}})} - \Pi_{(\alpha_s, \delta_s, \theta_{\text{um}})})$. The final intensity profile of the system *star + spot* is thus:

$$\begin{aligned} & I_\star(\mu) \Pi_{(0,0,\theta_\star)} \\ & - (I_\star(\mu_s) - I_{\text{pen}}) (\Pi_{(\alpha_s, \delta_s, \theta_{\text{pen}})} - \Pi_{(\alpha_s, \delta_s, \theta_{\text{um}})}) \\ & - (I_\star(\mu_s) - I_{\text{um}}) \Pi_{(\alpha_s, \delta_s, \theta_{\text{um}})} \end{aligned} \quad (2)$$

The corresponding complex visibility calculation is presented in Annex A.2. Interferometers cannot see such details as penumbra, and we thus ignore it for the rest of this study. Its intensity is set to $I_{\text{pen}} = I_\star$ and its diameter to $\theta_{\text{pen}} = 0$. To calculate the spot's intensity $I_s = I_{\text{um}}$, we consider it as a black body. We thus calculate the spectral radiance of a spot with Planck's law, that depends on the spot's temperature at the chosen wavelength. We normalize it with the star's radiance (also considered as a black body) to get the spot's intensity such as $0 < I_s < 1$ as needed in the complex visibility equation.

2.3. Model of a transiting exoplanet and a spot

The last case to be studied is a star with a transiting exoplanet and a spot. We make the hypothesis that the exoplanet and the spot's projected surfaces on the stellar surface do not overlap, i.e. $N' \neq N$ with $N = \cos(2\pi(u\alpha_p + v\delta_p)) + i \sin(2\pi(u\alpha_p + v\delta_p))$ and $N' = \cos(2\pi(u\alpha_s + v\delta_s)) + i \sin(2\pi(u\alpha_s + v\delta_s))$, and that both are located inside the stellar disk.

Merging the two previous models, the intensity profile of the system *star + exoplanet + spot* is:

$$\begin{aligned} & I_\star(\mu) \Pi_{(0,0,\theta)} - (I_\star(\mu_p) - I_p) \Pi_{(\alpha_p, \delta_p, \theta_p)} \\ & - (I_\star(\mu_s) - I_{\text{pen}}) (\Pi_{(\alpha_s, \delta_s, \theta_{\text{pen}})} - \Pi_{(\alpha_s, \delta_s, \theta_{\text{um}})}) \\ & + (I_\star(\mu_s) - I_{\text{um}}) \Pi_{(\alpha_s, \delta_s, \theta_{\text{um}})} \end{aligned} \quad (3)$$

The corresponding complex visibility calculation is presented in Annex A.3.

3. Detecting a transiting planet or a spot

3.1. Impacting parameters

We first performed simulations to estimate the minimum baseline length (MBL) needed to obtain a given signal on the interferometric observables. We have explored the parameters space that can impact the MBL, either for phases or squared visibilities: exoplanet's diameter, stellar diameter, spot's temperature and exoplanet location. However, all parameters but one has to be fixed in order to study its specific impact on the MBL. Thus, the nominal values of the parameters, when their impact on the MBL is not tested, are given on Tab. 1. The star's diameter ($\theta_\star = 1$ mas) is chosen to be easily resolved in the visible wavelength with baselines of ~ 300 m and roughly corresponds to F, G, K stars

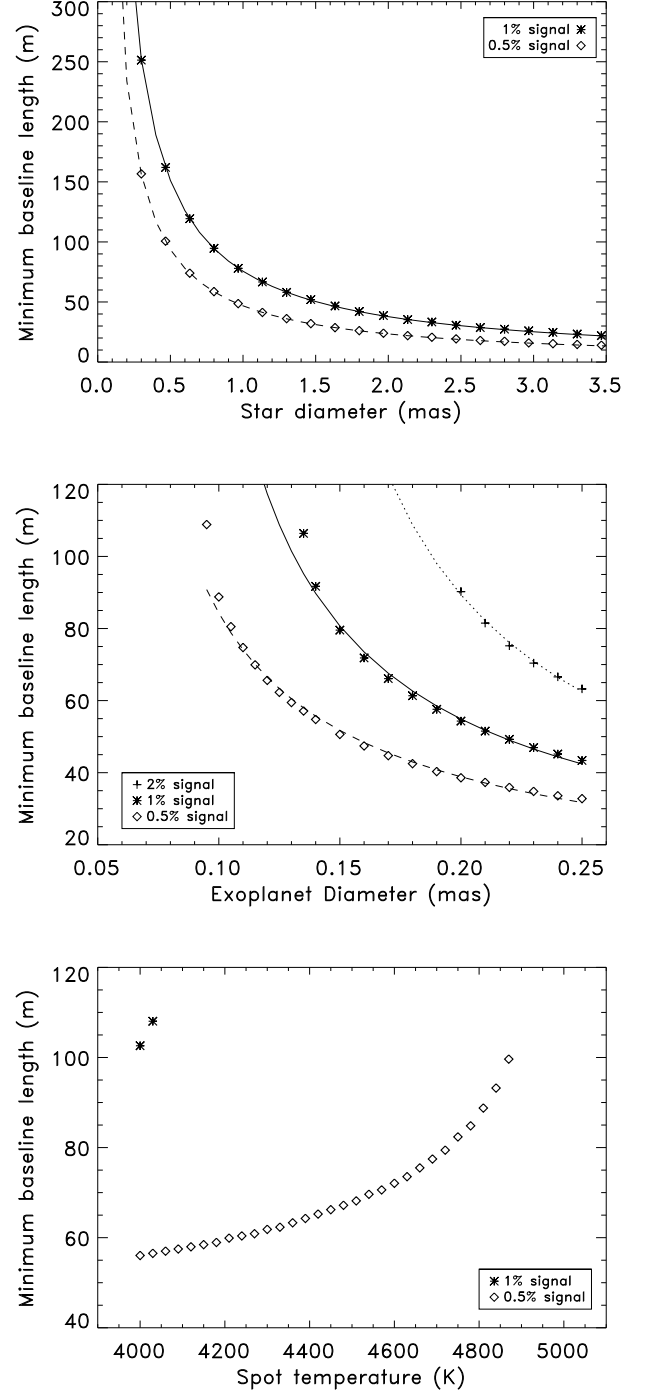


Fig. 1: Squared visibilities. The MBL is calculated for variations of 2%, 1% and 0.5% (crosses, asterisks and diamonds, respectively) as a function of three parameters: *Top*: star's diameter with $\theta_p/\theta_\star = 0.15$ and $(\alpha_p = 0.2\theta_\star, \delta_p = 0)$ mas. *Middle*: exoplanet's diameter with $\theta_\star = 1$ mas and $(\alpha_p = 0.2, \delta_p = 0.0)$ mas. *Bottom*: spot's temperature for $\theta_s = 0.15$ mas and $(\alpha_s = 0.2, \delta_s = 0.0)$ mas. The curves in the upper panel correspond to the analytical formula (see text). The curves in the middle panel correspond to the fit of Eq. 7.

around which exoplanets have been found until now (see e.g. Ligi et al. 2012). The exoplanet and spot location on the stellar disk are the same: $(\alpha_{p,s} = 0.2, \delta_{p,s} = 0)$. The exoplanet's diame-

ter corresponds to the upper limit of existing exoplanets' angular diameters (see Sec. 5).

Parameter	Fixed Value
θ_\star	1 mas
T_\star	5500 K
θ_p	0.15 mas
θ_s	0.15 mas
T_s	4300 K

Table 1: Values of the parameters when their impact on the MBL is not tested.

We have chosen realistic variation domains for each parameters. They are given in Tab. 2. The upper limit of the exoplanet's diameter goes beyond the generally known exoplanets' angular diameters, and would rather correspond to a brown dwarf, but a signal corresponding to such a large object on interferometric observables would allow disentangling between a planetary and a stellar companion. When testing the star's diameter impact, the ratio θ_p/θ_\star is steady and equal to 0.15, acting like the same system was seen at different distances, otherwise two parameters would vary at the same time (the star's diameter and the exoplanet's one). The exoplanet's location is proportional to the star's diameter, i.e. ($\alpha_p = 0.2 \times \theta_\star$, $\delta_p = 0.0$). The spot's temperature variation is set according to Strassmeier (2009); Berdyugina (2005).

3.2. Absolute or relative variation of signal

We first consider the absolute variations induced by exoplanets and magnetic spots on interferometric observables, i.e.: $|V_{p+\star}^2 - V_\star^2| > S$, where V_\star is the visibility modulus of the star alone. This means that the accuracy required to detect exoplanets or spots should be higher than the variation induced. We calculate the MBL for $S = 0.5\%, 1.0\%, 2.0\%$. Searching a smaller variation would be unrealistic as interferometers hardly reach such an accuracy. We made preliminary calculations of the MBL to identify the reachable upper limit of the signal and found no solution for better precisions than 2.0%. The variation of the MBL according to the different parameters is presented on Fig. 1. For the phases, we selected variations of 2° and 20° , which are shown on Fig. 2, and from which it could be possible to derive closure phase values.

But this first approach is really conservative as it implicitly considers that the visibility measurements are not limited by photon noise but by a fixed noise. If we consider that the signal to noise ratio of a measurement is just photon-noise limited then the uncertainty σV^2 can be written as:

$$\sigma V^2 = \frac{V^2}{SNR}. \quad (4)$$

Thus in a second step we compute the MBL for two values of the signal to noise ratio: 20 for good observing conditions and 5

Parameter	Variation domain
θ_p	0.04 – 0.24 mas
α_p	0 – 0.30 mas
θ_\star	0.30 – 3.35 mas
T_s	4000 – 5170 K

Table 2: Variation domain of the parameters when their impact on the MBL is tested.

for limit conditions. This means that we calculate the MBL such as :

$$\frac{|V_p^2 - V_\star^2|}{V_\star^2} > \frac{1}{SNR} \quad (5)$$

The variation of the MBL considering the different SNR are presented on Fig. 3.

3.3. Results

Table 3 is a summary of the main results. It describes the most interesting values of the MBL obtained for the different parameters. Thus, it gives the MBL obtained for the minimum tested exoplanet's diameter, star's diameter, maximum tested spot's temperature and the MBL corresponding to the exoplanet's position. For this last parameter, an average of the MBL is given since it is almost constant.

The analytic expression of the complex visibility is a function of $z = \pi \theta_\star B / \lambda$ only, so we expect the MBL to be proportional to θ_\star^{-1} (and to λ). This is indeed the case as shown in the upper panel of Fig. 1, where the data points are given by COMETS and the lines are $76/\theta_\star$ (solid line) and $47/\theta_\star$ (dashed line). The same behavior is observed on the top right panel of Fig. 2, where we see that baselines larger than 350 m are necessary to detect the planet on phases. The MBL are slightly higher for a spot than for an exoplanet (for example, in the case of a 4300 K spot, we find that MBL of 401 m and 604 m are necessary to get signals of 2° and 20° respectively for $\theta_\star = 0.3$ mas).

Spots of temperature $T = 5170$ K (the maximum tested value) can also be detected on phases and considering the two chosen SNRs. However, there is no detectable absolute signal of 2% due to the spot, and there are solutions only for $T_s < 4030$ K, which defines the upper limit to get an absolute signal of 1% in this study.

The exoplanets' diameter has a strong impact on the MBL. Even under bad conditions ($SNR = 5$), a small exoplanet ($\theta_p = 0.04$ mas) can be detected with hectometric baselines. However, there is no detectable absolute variation of the squared visibility for small exoplanets ($\theta_p < 0.09$ mas for a signal of 0.5%).

According to this model, baselines that already exist should be long enough to detect exoplanetary or spot signals on visibilities, if the exoplanet is large enough or the spot dark enough (with a low temperature). To detect small exoplanets or hotter spots, phase measurements are more appropriate as their signal reach low but still detectable values (like 2°). For the same diameter, the MBL needed to detect a spot is larger than for an exoplanet, because of its contrast with the star, that is more important in the case of the exoplanet. An exoplanet provokes a higher signal on interferometric observables that is thus easier to detect. For large enough stars ($\theta > 0.3$ mas), CHARA baselines are already large enough to detect a certain variation of the interferometric observables due to the presence of exoplanets or spots. The problem actually lies in instrument's accuracy (see next Section).

Finally, from these results, one can easily derive a general empirical formula allowing to compute the MBL. The difference between the reference and perturbed squared visibilities reads :

$$\left| \left(\frac{\tilde{I}_\star + \tilde{I}_p}{\tilde{I}_\star(0) + \tilde{I}_p(0)} \right)^2 - \left(\frac{\tilde{I}_\star}{\tilde{I}_\star(0)} \right)^2 \right|.$$

The perturbing body can be detected if and only if this difference is larger than S . Expanding to first order, one finds that it is

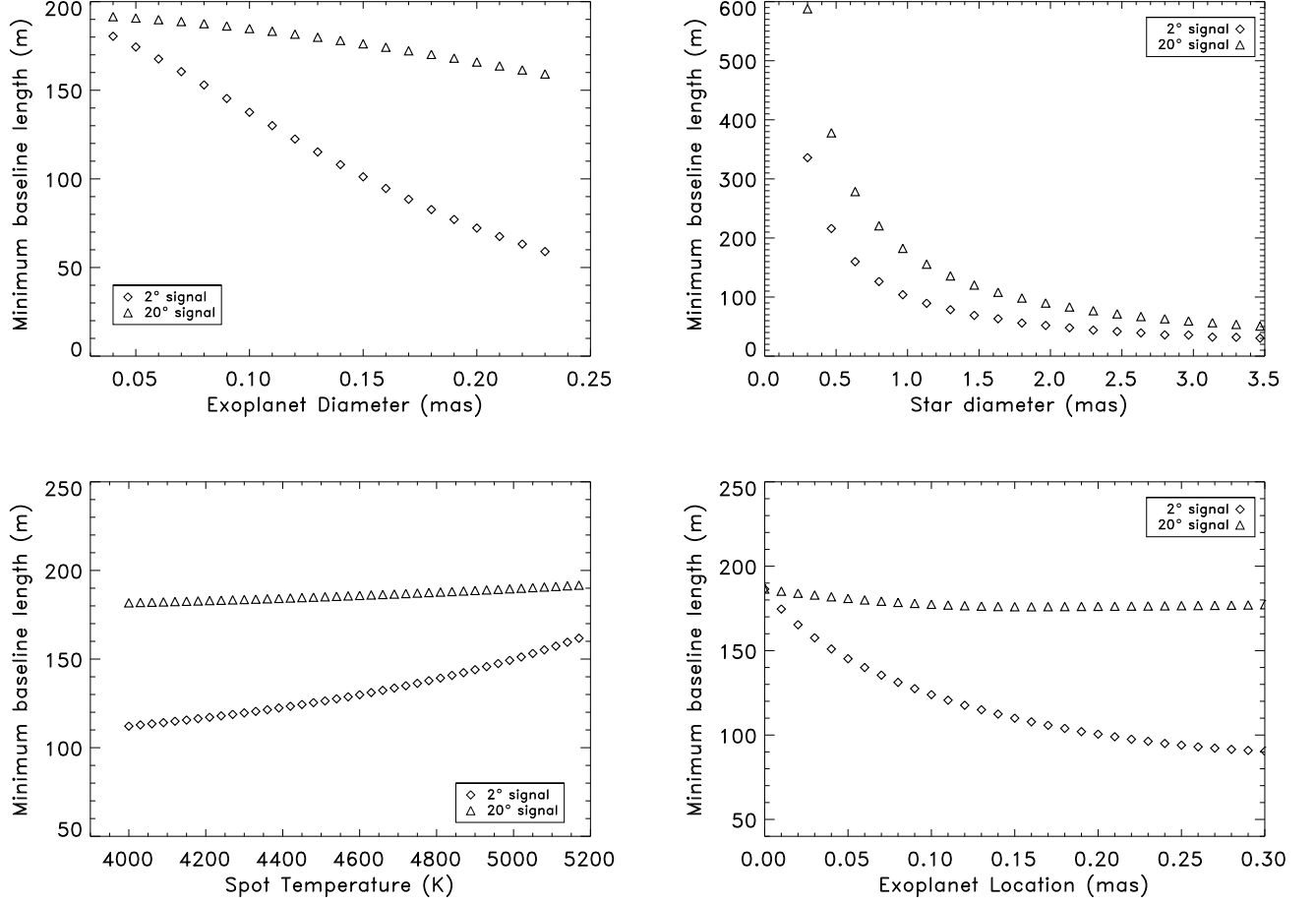


Fig. 2: Phases. Variations of the MBL according to different parameters, with the same fixed parameters as in Fig. 1. *Top*: the impacting parameters are the exoplanet’s diameter (left) and the star’s diameter (right). *Bottom*: the impacting parameters are the spot temperature (left) and the exoplanet location on the stellar disk (right), for which $\theta_p = 0.15$ mas. MBL are calculated for 20° (triangles) and 2° (diamonds) variations.

	Visibility					Phases	
	0.5%	1%	2%	SNR = 5	SNR = 20	2°	20°
θ_*	0.3 mas 160 m	0.3 mas 250 m	/	0.3 mas 515 m	0.3 mas 364 m	0.3 mas 340 m	0.3 mas 600 m
θ_p	0.09 mas 110 m	0.14 mas 110 m	0.20 mas 90 m	0.04 mas 190 m	0.04 mas 180 m	0.04 mas 180 m	0.04 mas 190 m
T_s	4870 K 100 m	4030 K 108 m	/	5170 K 175 m	5170 K 158 m	5170 K 184 m	5170 K 192 m
α_p	C 46m	C 73 m	C 250 m	C 155	C 110 m	0.3 mas 90 m	0.3 mas 180 m

Table 3: Summary of the results obtained for the MBL tests. For each tested parameter are indicated the minimum or maximum value of our test for which a MBL is found, and the value of the corresponding MBL (see text). C stands for constant.

equivalent to :

$$\frac{\theta_p}{\theta_*} < \sqrt{\frac{S}{2}}. \quad (6)$$

This means that the exoplanet’s angular diameter has to be larger than $\theta_{\min} = \sqrt{\frac{S}{2}} \times \theta_*$ to be detected. Therefore, we can look for a general formula of the form $MBL = \Gamma(\theta_*, S, \lambda) \left(\frac{\theta_p}{\theta_*} - \sqrt{\frac{S}{2}} \right)^{\Delta(S)}$. As we have seen in Sec. 3.3, Γ must be proportional to λ/θ_* . We

find the dependence of Γ and Δ on S by least squares method to find that the best fit is :

$$MBL = (17 \times S^{0.1}) \times \left(\frac{\theta_p}{\theta_*} - \sqrt{\frac{S}{2}} \right)^{-1.7 \times S^{0.2}} \times \left(\frac{\theta_*}{1 \text{ mas}} \right)^{-1} \times \frac{\lambda}{720.10^{-9} \text{ m}} \quad (7)$$

This law is plotted on Fig. 1 (solid, dashed and dotted lines, middle panel). It gives a good fit of the MBL.

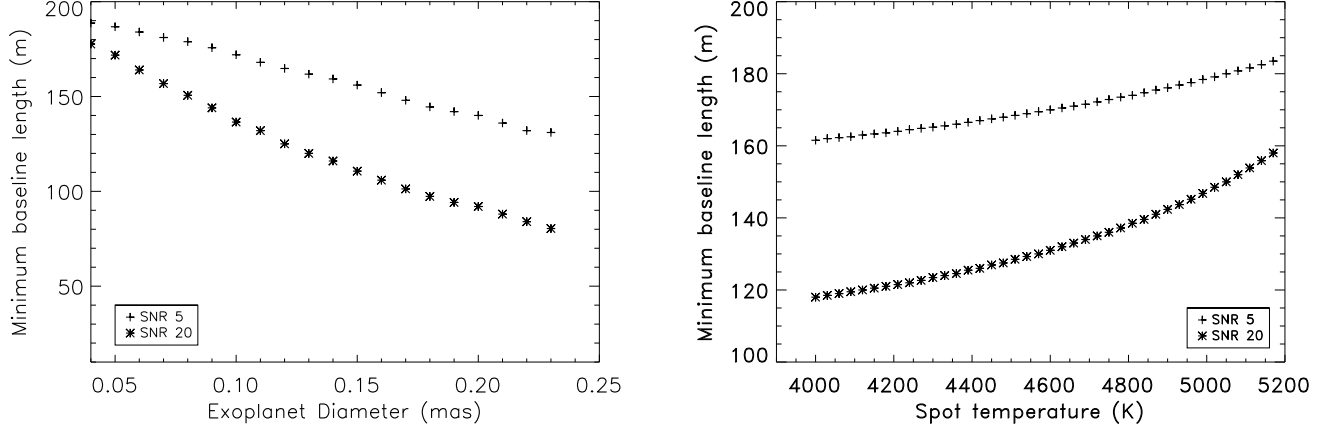


Fig. 3: Variations of the MBL considering the relative errors on squared visibilities according to the exoplanet’s diameter (top) and the spot’s temperature (bottom). We consider SNR of 5 (crosses) and 20 (asterisks) and the same fixed parameters as in Fig. 1.

As an example, we have taken the transited host star HD189733, which angular diameter is $\theta_\star = 0.38$ (Baines et al. 2008) and whose transiting exoplanet’s angular diameter is $\theta_p = 0.056$ mas, derived from the combination of its linear radius (Torres et al. 2008) and the star’s distance (van Leeuwen 2007). At $\lambda = 720$ nm, we find with the formula $MBL = 218$ m for a signal of 1%, and $MBL = 454$ m for a signal of 2%. As expected, since the angular resolution is $\propto B/\lambda$, with B the baseline, these values are greatly lower than in the infrared domain. For the same star, signals of 1% and 2% in the K band ($2.13\mu\text{m}$) would be reached with $MBL = 645$ m and $MBL = 1344$ m, respectively. Since we only consider transiting exoplanets, the difference of contrast (visible versus infrared) between an exoplanet and its host star does not change the results.

3.4. Discussion

Knowing at which spatial frequency (and thus in which visibility lobe) an exoplanet/spot signal is detectable will bring information on the sensitivity limit that interferometers have to provide to make such measurements, including phase and closure phase ones. For three different spatial frequencies corresponding to the middle of the first lobe of visibility (1.1×10^8 1/rad), close to the first null (2.1×10^8 1/rad) and in the middle of the second lobe (3.4×10^8 1/rad), the maximum, minimum and median differences between the squared visibility of a transited star and a single star are computed, along with the maximum and median differences in phase (the minimum difference is zero and is not represented). They are tested according to the exoplanet’s diameter as this parameter induces strong variations of the MBL as shown in Sec. 3. They include the complete (u, v) plane. Fig. 4 shows for each of these three cases the level corresponding to 2%, 1% and 0.5% absolute differences (solid lines) and relative variations for SNR of 20 and 5 (dashed lines). It also provides the levels 2° (red) and 20° (blue) for phases.

In the first lobe of visibility, the highest difference between both visibilities (2%) happens for $\theta_p > 0.20$ mas, which does not correspond to an exoplanet’s diameter but rather a brown dwarf’s. Even a good SNR cannot provide a sufficient signal to detect an exoplanet (solution for $\theta_p > 0.22$ mas for the red dashed line). However, there is a maximum absolute signal of

0.5% and 1% on squared visibilities for exoplanets’ diameters such as $\theta_p > 0.10$ mas and $\theta_p > 0.15$ mas respectively, which correspond to real cases. The signal on the phase measurement only reaches 2° for $\theta_p > 0.17$ mas, which is almost the highest limit for a planet representation.

The visibilities show bigger differences close to the zero of visibility and in the second lobe when considering relative errors. For SNR= 20, very small exoplanets ($\theta_p > 0.08$ mas for the smallest) generate a variation of the visibility that can be detected close to the zero of visibility, and exoplanets as small as $\theta_p = 0.04$ mas generate variations able to be measured in the second lobe. In bad conditions (SNR= 5), small exoplanets can still be detected. The smallest ones are such that $\theta_p > 0.16$ mas and $\theta_p > 0.10$ mas for the first zero of visibility and in the second lobe respectively. This shows that a real opportunity of exoplanets detection is possible with interferometry.

Absolute variations of the visibility exist anyway close to the zero and in the second lobe, but are found for bigger planets compared to relative errors. To get a 1% signal, exoplanet’s diameter have to be $\theta_p > 0.17$ mas. However, a maximum signal of 0.5% is detectable for only $\theta_p > 0.13$.

Thus, if focusing on relative differences, which take into account the SNR and thus gives a real observing condition, signals of small exoplanets can be identified near the first zero of visibility and in the second lobe. For each frequency, they never allow to detect very small exoplanets ($\theta_p < 0.05$ mas) for these considered signals. The sensitivity of instruments is thus a fundamental parameter to be improved.

The SNR is lower when measuring low visibilities, like close to the first zero of visibility and in the following lobes. It is however where the higher order measurements (phase or closure phase) show an evidence of the presence of the exoplanet or spot, i.e. a maximum signal. In our study, the phase signal reaches 2° for a star with an exoplanet of diameter $\theta_p > 0.08$ mas and $\theta_p > 0.06$ mas close to the zero and in the second lobe respectively. This is also where planetary companions are able to cause a phase variation of 20° , but this only concerns big planets ($\theta_p > 0.25$ and $\theta_p > 0.17$ mas respectively). Thus, taking the SNR into account tells us if the signal of the exoplanet or the star can also be measured via these higher order observables.

Table 4 displays the accuracy reached by several instruments on CHARA, NPOI and the VLTI, that can be found in the littera-

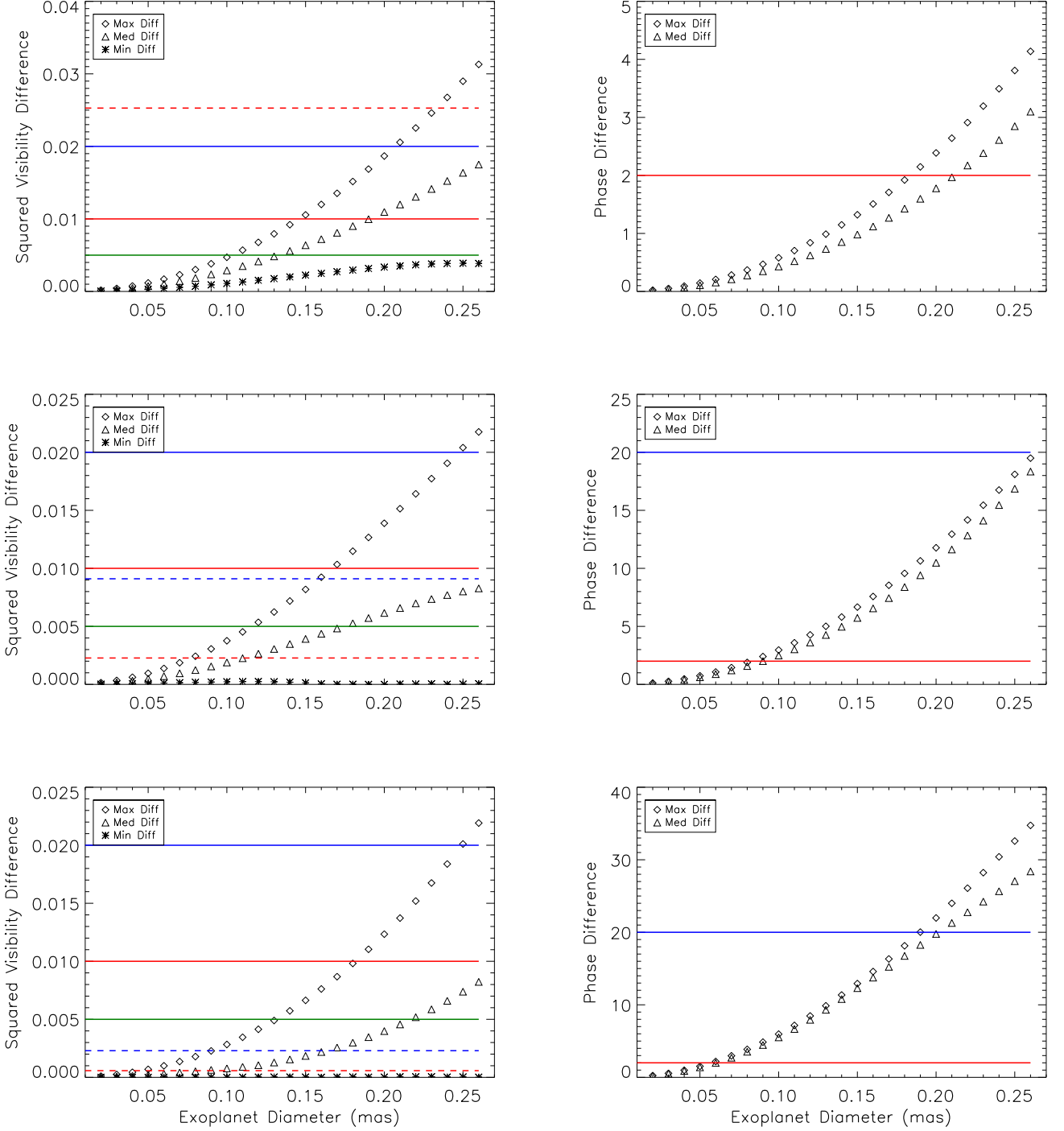


Fig. 4: Squared visibility and phase differences between a 1 mas star with a transiting exoplanet at (0.2,0.0) and a single star at different spatial frequencies (1.1×10^8 (1/rad); top, 2.1×10^8 (1/rad); middle, 3.4×10^8 (1/rad); bottom). Squared visibilities : *Solid lines* : Absolute errors (1%; red, 2%; blue, 0.5%; green). *Dashed lines* : Errors corresponding to different SNR : 5 (blue) and 20 (red). Phases (in degree) : 2° (red) and 20° (blue).

ture or that are extracted from Chiavassa et al. (2014). It is difficult to link instrumental precisions, that for most of them depend on particular cases, with a general conclusion on the feasibility of exoplanet characterization. However, comparing Tab. 4 with the information provided by the Fig. 4, we can notice that :

- for most of instruments, the accuracy on the squared visibility is not sufficient to detect small exoplanets ($\theta_p < 0.10$ mas under good observing conditions). JouFLU could be a good candidate, but the expected 0.1% accuracy is not enough in its wavelength range (K' band). Instruments' accuracy have

Instrument	V^2 accuracy	CP accuracy	Ref.
VEGA/CHARA	1 – 2%	-	1
FLUOR/CHARA	0.3%	-	2
JouFLU/CHARA	0.1%*	-	3
	1%	-	4
VISION/NPOI	5 – 20%**	1 – 10°	5
CLIMB/CHARA	5%	0.1°	6
CLASSIC/CHARA	5%	-	7
PAVO/CHARA	~ 5%	5°	8
MIRC/CHARA	~ 2%	< 1°	9
	-	0.1 – 0.2	10, 11, 12
AMBER/VLTI	-	0.20 – 0.37	13
PIONIER/VLTI	-	0.25 – 3°	14
	3 – 15%	0.5°	15
GRAVITY/VLTI	-	1	16
MATISSE/VLTI	1.6 – 2.3%	< 1.16	17

Table 4: Summary of the accuracy reached on squared visibilities V^2 and closure phases (CP) by different instruments.

*Expected on visibility modulus **On visibility amplitude.

Ref.: ¹Mourard et al. (2009) ²Coudé du Foresto et al. (2003) ³Scott et al. (2013) ⁴Lhomé et al. (2012) ⁵Garcia et al. (2014) ⁶ten Brummelaar et al. (2012) ⁷McAlister et al. (2012) ⁸Maestro et al. (2012) ⁹Che et al. (2012) ¹⁰Zhao et al. (2011) ¹¹Zhao et al. (2010) ¹²Zhao et al. (2008) ¹³Absil et al. (2010) ¹⁴Absil et al. (2011) ¹⁵Le Bouquin et al. (2011) ¹⁶(Chiavassa et al. 2014, Final Design Review 2011, private communication) ¹⁷Lopez (2012).

to improve by a factor 10 to be able to characterize exoplanets.

- the accuracy on CP is generally reached with measurements on the first lobe of visibility, and cannot be measured beyond (because of the wavelength or instrument sensitivity). If this accuracy is reached for measurements beyond the first null, then exoplanets characterization could be achieved.

4. Detecting a transiting planet in presence of stellar activity noise

The impact of an exoplanet and a spot on interferometric observables have been discussed separately, and the impacting parameters are now known. We now want to explore the effect of a spot on the characterization of a transiting exoplanet.

Figure 6 (upper panels) shows the difference between the visibility of a single star and a star with an exoplanet and/or a spot, i.e. the absolute signal induced by these components.

The left panel represents the signal induced by an exoplanet alone, with diameter and position are $\theta_p = 0.10$ mas and (0.2, 0.0) (in mas). On the two other panels, we add a spot of diameter $\theta_s = 0.10$ mas at the position (0.2, 0.2). On the middle panel, $\theta_p = 0.10$ mas and on the right panel, $\theta_p = 0.05$ mas. This is represented on Fig. 5. If the accuracy of interferometers reaches the signal induced by both spot and exoplanet, their presence may affect the determination of star's angular diameter, as they are generally measured in this visibility lobe. But this would also mean that a simple limb-darkened representation of the star would not be accurate anymore (see e.g. Lacour et al. 2008). At higher spatial frequencies, the interferometric signal becomes more sensitive to small structures (spots, granulation patterns) and 3D models from RHD atmospheric simulations become essential to fit the interferometric data (see e.g. Bigot et al. 2006; Lacour et al. 2008; Chiavassa et al. 2012, 2014). Using those models is another solution to take into account the stellar

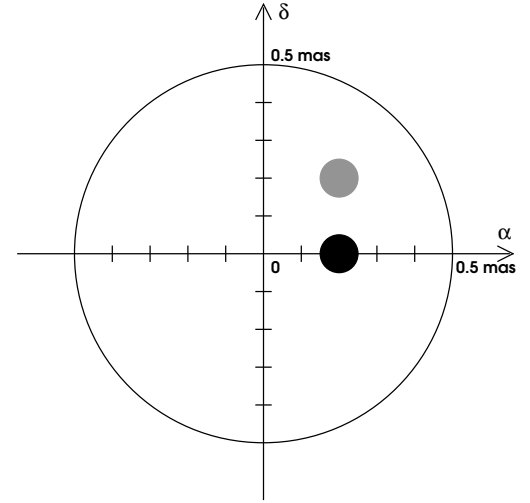


Fig. 5: Representation of the configuration of the system studied in Sec.4 for the case $\theta_p = 0.10$ mas at (0.2, 0.0) mas and $\theta_s = 0.10$ mas at (0.2, 0.2) mas. The black disk represents the exoplanet and the grey disk represents the spot.

activity (in terms of stellar granulation) that also affects interferometric observables.

Figure 6 (bottom panels) shows the corresponding phases. Again, the star with a spot and/or an exoplanet has a different signal from a single star's, that vary according to the observing direction and sizes of the additional objects (the phase of a single star is $0 \pm 180^\circ$). When the spot and the exoplanet have the same size, the exoplanet's signal is mixed up with the spot's signal until the 2nd lobe. When the exoplanet is smaller than the spot, the signal on the phase is totally disturbed by the spot, and their signal is already detectable from the 2nd lobe. The exoplanet's signal is thus hard to extract.

For both cases, not taking into account the spot leads here to a bad interpretation of the signal, like a bigger transiting planet, and highlights the necessity of observing the star out of the transit to characterize the stellar activity, that could be subtracted from the signal recorded during the transit time to allow the characterization of the exoplanet. Other effects should not be forgotten, like the granulation as shown by Chiavassa et al. (2014) who use a realistic three-dimensional radiative hydrodynamical simulations obtained with the Stagger-Grid (Magic et al. 2013). It perturbs closure phase measurements in particular from the third lobe of visibility. However, this would be possible to characterize a Hot-Jupiter; the characterization of an Earth-like planet could require a much higher sensitivity.

5. Discussion : exoplanet's detection applied to CHARA and the VLTI

To evaluate the actual number of potential interferometric targets, and relying on the results of previous sections, we have to take into account the host star's angular diameter and the ratio θ_p/θ_* , as well as the stellar magnitude in the considered wavelength. Fig. 7 shows all the transiting exoplanets host stars with available angular diameters according to the ratio θ_p/θ_* . Among the ~ 400 transiting exoplanets known today¹, only half of their parent's star have a known distance and/or known radius, which

¹ January 2014

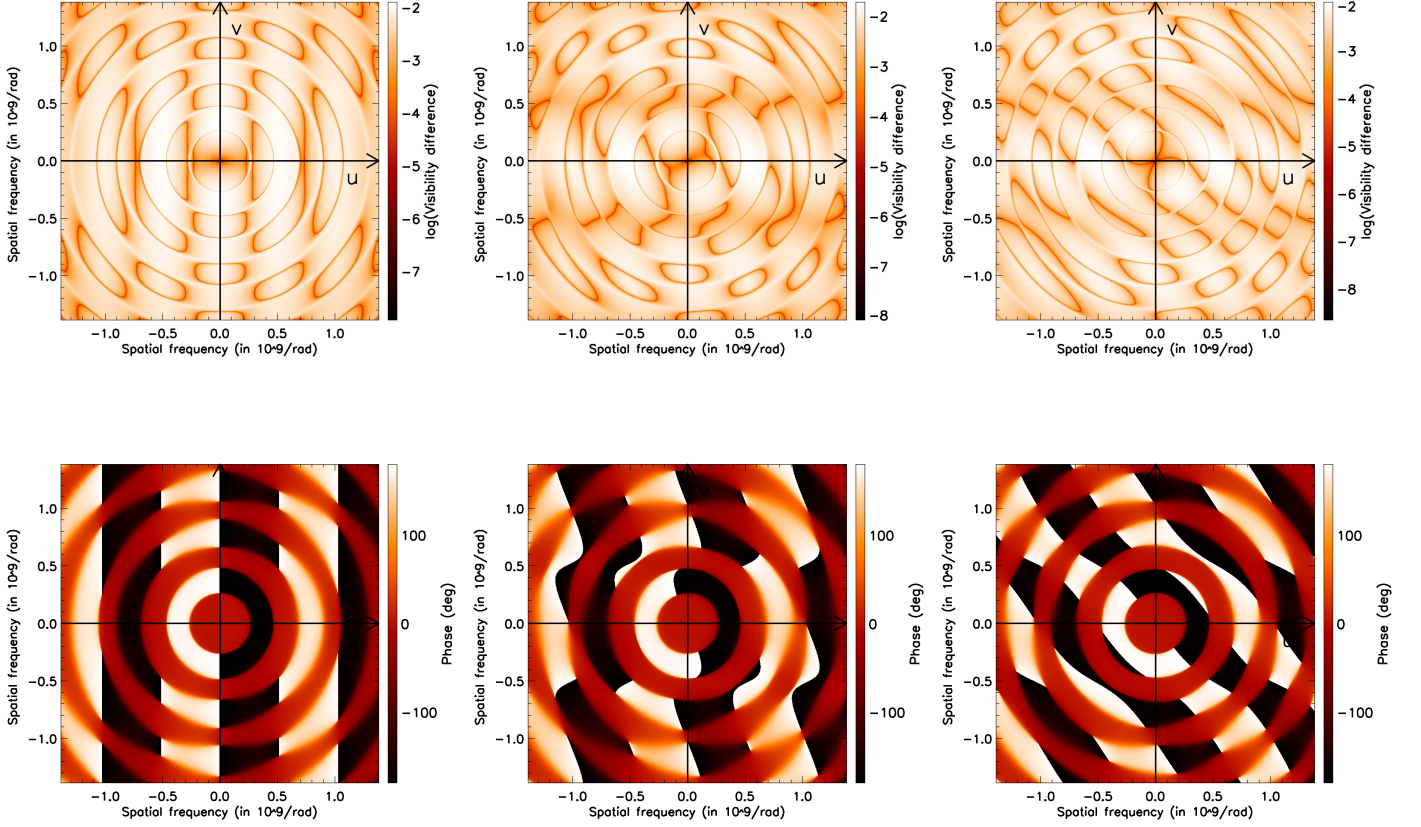


Fig. 6: Map of the signal induced by an exoplanet at (0.2, 0.0) and a spot at (0.2, 0.2) on the visibility modulus (log scale, upper panels) and the phases (bottom panels), for a 1 mas star. *Left*: exoplanet alone with $\theta_p = 0.10$ mas. *Middle*: exoplanet of diameter $\theta_p = 0.10$ mas with a spot of diameter $\theta_s = 0.10$ mas. *Right*: Same as middle with $\theta_p = 0.05$ mas.

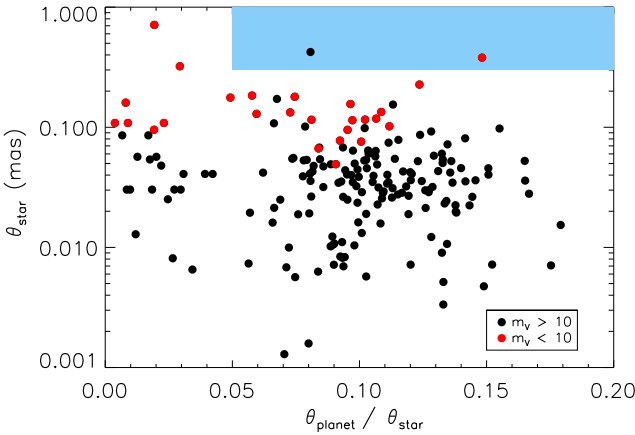


Fig. 7: Transiting exoplanets host stars with available distance and radius allowing to derive their angular diameter. They are plotted according to the ratio θ_p/θ_\star . In red are the stars with $m_V < 10$ and in black $m_V > 10$. The blue box represents VEGA's current detectability.

reduces the number of known angular diameter of transiting exoplanets host stars to 188.

Most of transiting exoplanets host stars have a diameter included between 0.005 and 0.20 mas. The maximum ratio θ_p/θ_\star is ~ 0.15 , with sparse exoplanets (or stars) having larger angular diameters. If the signature of exoplanets as small as $\theta_p = 0.05$ mas can be detected with baselines smaller than 200 m under a high SNR (see Fig.3 and Fig. 4), the angular resolution already represents an important limitation in the detection of the star's planetary companion. Since the visible domain provides a better angular resolution compared to the infrared one at similar baseline, interferometers operating in the visible wavelength appear more suitable. The CHARA array (McAlister et al. 2012) holds the longest baselines in the world (up to 330 m), and hosts many instruments, among them VEGA (Mourard et al. 2009; Ligi et al. 2013) and PAVO (Ireland et al. 2008) operating in the visible, and thus benefit from the best angular resolution in the world (~ 0.3 mas), despite a limiting magnitude in the V band around ~ 8 . However, this resolution remains in principle too low as most of transiting exoplanets host stars have even smaller angular diameters. However, through phase only measurements, preliminary detections are possible in some very specific cases. The NPOI is also a good candidate to characterize exoplanets, as it operates in the optical wavelength. Its baselines are for now too small to reach a high enough angular resolution (the maximum baseline length is currently 79 m), but it should be the case within the next year (Baines et al. 2014).

On the contrary, the VLTI does not own baselines larger than ~ 130 m, and since it mainly hosts instruments operating in the infrared domain, no instrument is able to reach such a resolution. Furthermore, Fig. 7 is affected by instrumental bias toward low magnitudes because of detection instruments, that is why the upper part is almost empty. Indeed, big surveys searching for exoplanets candidates were generally focused on faint stars (*Kepler*, *CoRoT*), which are too faint to be observed by actual interferometers. Future missions should allow to fill this part of the diagram. SPHERE (Beuzit et al. 2007), a new instrument being developed for the VLT, should detect Giant planets around bright stars by direct imaging but these planets will be rather far away from the stars, making the probability of transit quite small; also SPHERE targets are mostly young stars, with enhanced levels of activity. Future missions like PLATO (Rauer & Catala 2012, $m_V < 11$), CHEOPS (Broeg et al. 2013, $m_V < 9$) or TESS (Ricker et al. 2010, $m_V < 12$) will target bright stars and complementary observations of those stars will become possible with interferometry and thus open new possibilities of exoplanets characterization with interferometry.

A few instruments are also being developed on CHARA and the VLTI. A new prototype of VEGA, called FRIEND (Bério et al., in prep), is currently being studied to reach a maximum angular resolution of 0.3 mas and be able to observe stars up to $m_V < 10$. They appear in red on Fig. 7. Assuming these improvements, we see that only one known star becomes a potential target for this study (they are included in the blue box; the star represented by a black dot is too faint). By only increasing the angular resolution of FRIEND by a factor of 3, resulting in a maximum spatial resolution of 0.1 mas, one can considerably increase the number of potential targets (by more than a factor of 10). The baseline lengths and the sensitivity have to be improved together to reach the core of potential detectable exoplanets.

6. Conclusion

We have computed the interferometric observables of a star with the new code COMETS and observed the variations induced by a transiting exoplanet and/or a magnetic spot on squared visibilities and phases. We show that several parameters of these objects affect the baseline length required to detect their signal, like the position, diameter or spot's temperature. Starting from the variation of the MBL as a function of the exoplanet's angular diameter, we have derived an analytical solution allowing to calculate the baseline length required to detect the absolute exoplanet's signature on squared visibilities. This directly shows the interest of using the visible wavelength over the infrared, and that visible interferometers are more adapted for exoplanet characterization. More importantly, current instruments use large enough baselines to reach the spatial angular resolution able to lead to a characterization of big exoplanets or very dark spots, but lack accuracy on squared visibility and phase (or CP) measurements.

To detect a 0.10 mas exoplanet crossing a 1 mas star at visible wavelength, an accuracy better than $\sim 0.5\%$ from the first null is required on squared visibilities, at best observing conditions. A precision better than $\sim 1^\circ$ on phases is necessary in the first lobe or better than $\sim 6^\circ$ in the second lobe. For now, no instrument can reach these accuracies. To detect a 0.05 mas exoplanet, the accuracy needed on squared visibilities and phases are $\sim 0.1\%$ and $\sim 1^\circ$ from the first null. Magnetic spots' signals can easily mimic these exoplanets' ones, and disentangling between both is essential for exoplanets characterization, but requires measurements generally beyond the 3^{rd} lobe of visibility.

Acknowledgements. We thank the anonymous referee, whose constructive remarks led to significant improvement of the paper. RL also acknowledges the Ph.D. financial support from the Observatoire de la Côte d'Azur and the PACA region and support from OCA after her Ph.D. This research has made use of The Extrasolar Planets Encyclopaedia at exoplanet.eu.

References

- Absil, O., Le Bouquin, J.-B., Berger, J.-P., et al. 2011, *A&A*, 535, A68
 Absil, O., Le Bouquin, J.-B., Lebreton, J., et al. 2010, *A&A*, 520, L2
 Armstrong, J. T., Mozurkewich, D., Rickard, L. J., et al. 1998, *ApJ*, 496, 550
 Baines, E. K., Armstrong, J. T., Schmitt, H. R., et al. 2014, *ApJ*, 781, 90
 Baines, E. K., McAlister, H. A., ten Brummelaar, T. A., et al. 2008, *ApJ*, 680, 728
 Baines, E. K., van Belle, G. T., ten Brummelaar, T. A., et al. 2007, *ApJ*, 661, L195
 Baron, F., Cotton, W. D., Lawson, P. R., et al. 2012, in *Society of Photo-Optical Instrumentation Engineers (SPIE) Conference Series*, Vol. 8445
 Berdyugina, S. V. 2005, *Living Reviews in Solar Physics*, 2, 8
 Beuzit, J.-L., Feldt, M., Dohlen, K., et al. 2007, in *In the Spirit of Bernard Lyot: The Direct Detection of Planets and Circumstellar Disks in the 21st Century*
 Bigot, L., Kervella, P., Thévenin, F., & Ségransan, D. 2006, *A&A*, 446, 635
 Broeg, C., Fortier, A., Ehrenreich, D., et al. 2013, in *European Physical Journal Web of Conferences*, Vol. 47, *European Physical Journal Web of Conferences*, 3005
 Che, X., Monnier, J. D., Kraus, S., et al. 2012, in *Society of Photo-Optical Instrumentation Engineers (SPIE) Conference Series*, Vol. 8445
 Chelli, A., Duvert, G., Malbet, F., & Kern, P. 2009, *A&A*, 498, 321
 Chiavassa, A., Bigot, L., Kervella, P., et al. 2012, *A&A*, 540, A5
 Chiavassa, A., Ligi, R., Magic, Z., et al. 2014, *A&A*, 567, A115
 Claret, A. & Bloemen, S. 2011, *A&A*, 529, A75
 Coudé du Foresto, V., Borde, P. J., Merand, A., et al. 2003, in *Society of Photo-Optical Instrumentation Engineers (SPIE) Conference Series*, ed. W. A. Traub, Vol. 4838, 280–285
 Duvert, G., Chelli, A., Malbet, F., & Kern, P. 2010, *A&A*, 509, A66
 Garcia, E., van Belle, G., Mutterspaugh, M. W., & Swihart, S. 2014, in *American Astronomical Society Meeting Abstracts*, Vol. 223, *American Astronomical Society Meeting Abstracts* #223, 154.26
 Howell, S. B., Rowe, J. F., Bryson, S. T., et al. 2012, *ApJ*, 746, 123
 Huber, D., Ireland, M. J., Bedding, T. R., et al. 2012, *MNRAS*, 423, L16
 Ireland, M. J., Mérand, A., ten Brummelaar, T. A., et al. 2008, in *Society of Photo-Optical Instrumentation Engineers (SPIE) Conference Series*, Vol. 7013
 Labeyrie, A., Allouche, F., Mourard, D., et al. 2012a, in *Society of Photo-Optical Instrumentation Engineers (SPIE) Conference Series*, Vol. 8445
 Labeyrie, A., Mourard, D., Allouche, F., et al. 2012b, in *Society of Photo-Optical Instrumentation Engineers (SPIE) Conference Series*, Vol. 8445
 Lacour, S., Meimon, S., Thiébaud, E., et al. 2008, *A&A*, 485, 561
 Le Bouquin, J.-B., Berger, J.-P., Lazareff, B., et al. 2011, *A&A*, 535, A67
 Leinert, C., Graser, U., Przygodda, F., et al. 2003, *Ap&SS*, 286, 73
 Lhomé, E., Scott, N., ten Brummelaar, T., et al. 2012, in *Society of Photo-Optical Instrumentation Engineers (SPIE) Conference Series*, Vol. 8445
 Ligi, R., Mourard, D., Lagrange, A. M., et al. 2012, *A&A*, 545, A5
 Ligi, R., Mourard, D., Nardetto, N., & Clausse, J.-M. 2013, *Journal of Astronomical Instrumentation*, 02, 1340003
 Lopez, B. 2012, *Publications de l'Observatoire Astronomique de Beograd*, 91, 129
 Maestro, V., Kok, Y., Huber, D., et al. 2012, in *Society of Photo-Optical Instrumentation Engineers (SPIE) Conference Series*, Vol. 8445
 Magic, Z., Collet, R., Asplund, M., et al. 2013, *A&A*, 557, A26
 Matter, A., Vannier, M., Morel, S., et al. 2010, *A&A*, 515, A69
 Mayor, M. & Queloz, D. 1995, *Nature*, 378, 355
 McAlister, H. A., ten Brummelaar, T. A., Ridgway, S. T., et al. 2012, in *Society of Photo-Optical Instrumentation Engineers (SPIE) Conference Series*, Vol. 8445
 Monnier, J. D., Berger, J.-P., Millan-Gabet, R., & ten Brummelaar, T. A. 2004, in *Society of Photo-Optical Instrumentation Engineers (SPIE) Conference Series*, ed. W. A. Traub, Vol. 5491, 1370
 Mourard, D., Clausse, J. M., Marcotto, A., et al. 2009, *A&A*, 508, 1073
 Nutzman, P. A., Fabrycky, D. C., & Fortney, J. J. 2011, *ApJ*, 740, L10
 Petrov, R. G. & AMBER Consortium. 2003, in *EAS Publications Series*, Vol. 6, *EAS Publications Series*, ed. G. Perrin & F. Malbet, 111
 Rauer, H. & Catala, C. 2012, in *EGU General Assembly Conference Abstracts*, Vol. 14, *EGU General Assembly Conference Abstracts*, ed. A. Abbasi & N. Giesen, 7033
 Ricker, G. R., Latham, D. W., Vanderspek, R. K., et al. 2010, in *Bulletin of the American Astronomical Society*, Vol. 42, *American Astronomical Society*

- Meeting Abstracts #215, 450.06
- Sanchis-Ojeda, R., Winn, J. N., Holman, M. J., et al. 2011, *ApJ*, 733, 127
- Scott, N. J., Millan-Gabet, R., Lhomé, E., et al. 2013, *Journal of Astronomical Instrumentation*, 02, 1340005
- Silva-Valio, A. & Lanza, A. F. 2011, *A&A*, 529, A36
- Strassmeier, K. G. 2009, *A&A Rev.*, 17, 251
- ten Brummelaar, T. A., Sturmman, J., McAlister, H. A., et al. 2012, in *Society of Photo-Optical Instrumentation Engineers (SPIE) Conference Series*, Vol. 8445
- Torres, G., Winn, J. N., & Holman, M. J. 2008, *ApJ*, 677, 1324
- Traub, W. A. & Jucks, K. W. 2002, *Washington DC American Geophysical Union Geophysical Monograph Series*, 130, 369
- van Belle, G. T., van Belle, G., Creech-Eakman, M. J., et al. 2008, *ApJS*, 176, 276
- van Leeuwen, F. 2007, *A&A*, 474, 653
- Zhao, M., Monnier, J. D., Che, X., et al. 2011, *PASP*, 123, 964
- Zhao, M., Monnier, J. D., Che, X., et al. 2010, in *Society of Photo-Optical Instrumentation Engineers (SPIE) Conference Series*, Vol. 7734
- Zhao, M., Monnier, J. D., ten Brummelaar, T., Pedretti, E., & Thureau, N. 2008, in *IAU Symposium*, Vol. 249, *IAU Symposium*, ed. Y.-S. Sun, S. Ferraz-Mello, & J.-L. Zhou, 71–77

Appendix A: Calculation of the complex visibility

A.1. Case of a transiting planet

We have calculated the 2D-Fourier transform (TF) of the intensity profile \tilde{I} . The normalized \tilde{I} gives the complex visibility. The resulting TF of the star's profile $\tilde{I}_\star(\rho)$ and of the exoplanet's profile $\tilde{I}_p(\rho)$ are :

$$\tilde{I}_\star(\rho) = I_\star(1) \frac{\pi \theta_\star^2}{4} \left(1 - \frac{b}{3}\right) \frac{[a J_1(z)/z + b(\pi/2)^{1/2} J_{3/2}(z)/z^{3/2}]}{(a/2 + b/3)} \quad (\text{A.1})$$

$$\tilde{I}_p(\rho) = \frac{\theta_\star}{2} \frac{J_1(\pi \theta_p \rho)}{\rho} \times \underbrace{\cos(2\pi(u\alpha_p + v\delta_p)) + i \sin(2\pi(u\alpha_p + v\delta_p))}_N, \quad (\text{A.2})$$

with $a = 1 - b$, $z = \pi \theta_\star \rho$ and $\rho = B_p/\lambda$, B_p being the projected baseline and λ the observing wavelength in nm. The spatial frequencies are represented by $u = \frac{B_x}{\lambda}$ and $v = \frac{B_y}{\lambda}$. The resulting complex visibility of the system is :

$$V_p(\rho) = [\tilde{I}_\star(\rho) - (I_\star(\mu_p) - I_p) \tilde{I}_p(\rho)] / \left[\frac{\pi}{4} \left(I_\star(1) \theta_\star^2 \left(1 - \frac{b}{3}\right) - (I_\star(\mu_p) - I_p) \theta_p^2 \right) \right]. \quad (\text{A.3})$$

A.2. Case of a spot

The normalized 2D-Fourier transform of Eq. 2 results in its complex visibility. The TF of the penumbra's and umbra's profiles are respectively \tilde{I}_{pen} and \tilde{I}_{um} :

$$\begin{aligned} \tilde{I}_{\text{pen}}(\rho) &= \frac{\theta_{\text{pen}}}{2} \frac{J_1(\pi \theta_{\text{pen}} \rho)}{\rho} \times N' \\ \tilde{I}_{\text{um}}(\rho) &= \frac{\theta_{\text{um}}}{2} \frac{J_1(\pi \theta_{\text{um}} \rho)}{\rho} \times N', \end{aligned} \quad (\text{A.4})$$

with $N' = \cos(2\pi(u\alpha_s + v\delta_s)) + i \sin(2\pi(u\alpha_s + v\delta_s))$. The TF of the star's profile is written in Eq. A.1. Combining these three TF gives the final complex visibility :

$$\begin{aligned} V_s(\rho) &= [\tilde{I}_\star(\rho) - (I_\star(\mu_s) - I_{\text{pen}}) \tilde{I}_{\text{pen}}(\rho) \\ &\quad + (I_{\text{um}} - I_{\text{pen}}) \tilde{I}_{\text{um}}(\rho)] / \\ &\quad \left[\frac{\pi}{4} \left(I_\star(1) \theta_\star^2 \left(1 - \frac{b}{3}\right) \right. \right. \\ &\quad \left. \left. - (I_\star(\mu_s) - I_{\text{pen}}) \theta_{\text{pen}}^2 + (I_{\text{um}} - I_{\text{pen}}) \theta_{\text{um}}^2 \right) \right]. \end{aligned} \quad (\text{A.5})$$

A.3. A transiting planet and a spot

The normalized TF of Eq.3 gives the complex visibility of the system. The TF of the exoplanet and spot profiles are calculated in Sec. 2.1 and 2.2 :

$$\begin{aligned} \tilde{I}_{\text{pen}}(\rho) &= \frac{\theta_{\text{pen}}}{2} \frac{J_1(\pi \theta_{\text{pen}} \rho)}{\rho} \times N' \\ \tilde{I}_{\text{um}}(\rho) &= \frac{\theta_{\text{um}}}{2} \frac{J_1(\pi \theta_{\text{um}} \rho)}{\rho} \times N' \\ \tilde{I}_p(\rho) &= \frac{\theta_p}{2} \frac{J_1(\pi \theta_p \rho)}{\rho} \times N \end{aligned} \quad (\text{A.6})$$

The final complex visibility is thus :

$$\begin{aligned} V_{p+s}(\rho) &= [\tilde{I}_\star(\rho) - (I_\star(\mu_p) - I_p) \tilde{I}_p(\rho) \\ &\quad - (I_\star(\mu_s) - I_{\text{pen}}) \tilde{I}_{\text{pen}}(\rho) \\ &\quad + (I_{\text{um}} - I_{\text{pen}}) \tilde{I}_{\text{um}}(\rho)] / \\ &\quad \left[\frac{\pi}{4} \left(I_\star(1) \theta_\star^2 \left(1 - \frac{b}{3}\right) - (I_\star(\mu_p) - I_p) \theta_p^2 \right. \right. \\ &\quad \left. \left. - (I_\star(\mu_s) - I_{\text{pen}}) \theta_{\text{pen}}^2 + (I_{\text{um}} - I_{\text{pen}}) \theta_{\text{um}}^2 \right) \right], \end{aligned} \quad (\text{A.7})$$

for which we use the squared modulus.